Fragmentation and Erosion of Two-Dimensional Aggregates in Shear Flow

Nikolina D. Vassileva, Dirk van den Ende,* Frieder Mugele, and Jorrit Mellema

Physics of Complex Fluids, Department of Science and Technology, Institute of Mechanics, Processes and Control—Twente, University of Twente, P.O. Box 217, 7500 AE Enschede, The Netherlands

Received August 25, 2006. In Final Form: November 28, 2006

We consider single two-dimensional aggregates containing glass particles trapped at a water/oil or water/air interface. Two modes for aggregate break up are observed: break up by fragmentation into a few parts and break up by erosion of single particles. We have studied the critical shear rate for these modes as a function of the aggregate size. Two different particle sizes were used. The smaller particles, with a radius of 65 μm, form aggregates that break up predominantly by erosion at a shear rate between 0.5 and 0.7 s^{-1}. This value hardly depends on the size of the aggregates. The larger particles, with a radius of 115 μm, form aggregates that break by erosion or by fragmentation. In both modes, the critical shear rate again depends only weakly on the size of the aggregates and ranges between 1.6 and 2.2 s^{-1}. Also the structural changes inside the aggregate before break up were studied. The aggregate behavior at the water/air and water/oil interfaces is quite similar. The critical shear rate for break up was also modeled. The model shows in both modes a weak dependence of the critical shear rate on the aggregate size, which is consistent with the experimental observations. The kinetics of the erosion process was also modeled and compared with the experimentally obtained time dependence of the aggregate size. The differences in the large and small particle systems can be attributed to the occurrence of friction forces between the particles, which one expects to be much larger for the large particle system, due to the stronger two-particle interaction.

1. Introduction

The behavior of aggregates is an important issue in liquid suspension processes. For example, in wastewater treatment, one needs an efficient method for the removal of particles.[1−4] Larger particles are easier to remove, thus it is convenient to work with aggregates of particles. Also, smaller flocs will settle down slower and will be captured less efficiently by air bubbles. Small flocs can also block the membranes during filtration. These processes are designed to minimize the breaking of flocs, but they can still be subjected to high shear rates (e.g., close to a mixing impeller or during the transfer from one tank to another), where the flocs have to resist the corresponding stresses.[4] Thus it is important to study aggregate behavior when subjected to flow in order to design efficient methods for their treatment.

Detailed knowledge of how three-dimensional (3D) aggregates will break is still missing. This is due to the complexity of the system and the involved processes: many-body interactions, irregular shapes, and the influence of contamination. Moreover, not all forces acting in these processes are clear.[4] The logical way to investigate such a complicated system is to start with the simpler two-dimensional (2D) case. In the 2D case, the influence of capillary forces on the structure formation is an interesting issue itself. The main advantage of 2D experiments is the absence of gravitational settling of the aggregates, which makes the visualization much easier. The theoretical modeling in two dimensions is also simpler. However, even for 2D systems, there is little information available on the break up mechanisms for different conditions. Floc break up has been classified in two general modes.[4,5] The first one is the removal of single particles or small aggregates from the parent aggregate, called surface erosion. In the second mode, the flocs break up into pieces with similar sizes, called fragmentation. The resulting size distribution after rupture can inform us whether erosion or fragmentation has occurred. Erosion produces fragments with much smaller size than the original aggregate, thus the particle size distribution is roughly bimodal.[6] The main qualitative difference between erosion and fragmentation is the energy input, which is low for erosion and high for fragmentation. The time scales of the two processes are also different. Fragmentation occurs immediately after applying the critical stress, while the erosion occurs over much longer time scales.[4] For 3D systems, there are indications that the two modes are driven by different stresses. Erosion is caused by shear in the tangential direction, and fragmentation is caused by a tensile stress acting normally across the floc.[7−9]

There is no unique way to determine the floc strength because the flocs can be very different in size, shape, and properties. It is also difficult to compare the results from different studies because the results depend strongly on the technique used for measuring the aggregate strength. Most researchers investigate the dependence of the floc size as a function of the applied hydrodynamic shear flow. For a review of the techniques used, we refer to Jarvis and co-workers.[3] The simplest way of evaluating the floc strength is to measure the ratio between the floc size before and after break up for a particular shear rate. The floc strength can be related to the energy dissipation of the system or the velocity gradient applied to the system. This technique

* Corresponding author. E-mail address: h.t.m.vandenEnde@tnw.utwente.nl.

(1) Wills B. A. *Mineral Processing Technology*; International Series on Material Science and Technology; Pergamon Press, Oxford, 1988; Vol. 41.

(2) Elimelech, M.; Gregory, J.; Jia, X.; Williams, R. A. *Particle Deposition and Aggregation*; Butterworth-Heinemann: Woburn, MA, 1998.

(3) Jarvis, P.; Jefferson, B.; Gregory, J.; Parsons, S. A. *Water Res.* **2005**, *39*, 3121.

(4) Ottino, J. M.; DeRoussel, H. S.; Khakhar, D. V. *Adv. Chem. Eng.* **1999**, *25*, 105.

(5) Parker, D. S.; Kaufman, W. J.; Jenkins, D. J. *Sanit. Eng. Div. Proc. Amer. Soc. Civ. Eng.* **1976**, *102* (EE2), 251.

(6) Redner, S. *Statistical Models for the Fracture of the Disordered Media*; Herrman, H. J., Roux, S., Eds.; Elsevier/North Holland: New York, 1990; p 321.

(7) Thomas, D. G. *AIChE J.* **1964**, *10*, 517.

(8) Mühle, K. *Coagulation and Flocculation*; Dobiáš, B., Ed.; Marcel Dekker: New York, 1993; p 355.

(9) Thomas, D. G. *AIChE J.* **1964**, *10*, 517.

10.1021/la0625087 CCC: $37.00
Published on Web 01/18/2007 PAGE EST: 9.4

relies upon complex theories and floc break up models. Recently developed techniques directly measure the floc rupture.[10−12] Pantina and Fust[10] investigated the bending of bonded colloidal particles using optical tweezers. The results show the existence of strong tangential forces between the particles, which they explain are from surface roughness. Yeung and Pelton[11] used micromechanical techniques to pull flocs apart. They found that break up occurs at the weakest spot inside the aggregate. This explains why a compact aggregate will break as a result of erosion. According to their results, the aggregate strength does not depend on the aggregate size.

In 2D experiments, most of the research has been concentrated on the investigation of particle monolayers at a liquid interface.[13−16] Aggregates in two dimensions were investigated by Hoekstra[17] and Hansen.[18] Hoekstra and co-workers[17] studied two systems of 2D suspensions with a different interaction potential. In one system, the particles could slide over each other, while, in the other system, they could not, depending on the attraction strength between the particles. They found that shear flow induces the same type of anisotropy in both systems. In the system with a strong attractive potential, the density inside the aggregates increases with the applied shear flow, while it decreases in systems with a weak attraction between the particles. Break up was found to occur at the weakest link in the aggregate (at a single contact point between the particles), and erosion was not observed. Hansen and co-workers[18] studied 2D colloidal aggregation in a Couette cell. The development of the cluster size and structure was followed at different shear rates. The weakly aggregated systems showed rearrangement into a more compact structure and a densification with increasing shear rate, while the strongly aggregated systems did not display a significant change in structure.

Analytical models can be used to describe the aggregate break up. These models generally oversimplify the aggregate structure. The two limiting cases are a uniform impermeable[19] or permeable[20] sphere. The model developed by Sontag and Russel[21] also considers a nonhomogeneous aggregate structure. The fracture of the aggregate is assumed to occur along planar surfaces (usually passing through the aggregate center)[19,22] or by crack growth.[23] The several models for break up predict a different dependence on the volume fraction and the radius of the primary particles.

Only a few studies dealing with erosion have been carried out.[4,24,25] Powell and Mason[24] described the erosion kinetics for compact spherical aggregates without attraction between the primary (cohesionless) particles. They found that the erosion rate depends on the flow type and the ratio between the aggregate and primary particle size, but it was independent of the shear rate.

In our previous study,[26] we presented experimental results for the break up of aggregates of glass particles (radius 115 μm) at a water/air (w/a) interface. An advantage of our experimental method is that it is direct and nondestructive. We observed with video microcopy single aggregates, which gave us a detailed look into the processes of breaking. In addition, the reverse process of aggregation after collision with another aggregate is suppressed, which also simplifies the analysis. However, the method has certain drawbacks, too. First, like every method looking at the single-particle level, it is difficult to get enough data for statistically significant results. Second, it was not possible to keep the aggregates in the field of view, and thus the exact moment of aggregate break up is seldom seen. To be able to collect statistically reliable data, we worked with aggregates consisting of submillimeter noncolloidal particles, which gave a similar initial structure for all experiments. Using noncolloidal particles has the advantage that we have a well-defined attraction force because the capillary force is significantly larger than the other forces. Our results showed that the aggregates break at nearly the same shear rate, independent of their size. The evolution of the aggregate before break up was also investigated. With increasing shear rate, the aggregates adopt a more circular shape, and the particles order in a denser hexagonal structure. A simple theoretical model was developed to explain the experimental data. In this model, it was assumed that the aggregate is a circular disk that will break along a center line into two equal pieces. We will name this "break up by fragmentation". The capillary and drag forces acting on both parts of the aggregate were calculated, and, from their ratio, the critical shear rate was found. The model shows a weak size dependence of the critical shear rate for break up, which is in agreement with the experimental observations.

Here we continue the investigation of 2D aggregate restructuring and break up using the techniques described in our previous paper.[26] We extend the experimental systems to two different interfaces (w/a and water/oil (w/o)) and two particle sizes (R_p = 115 and 64 μm), varying in this way both the particle−particle interaction and the hydrodynamic forces on the particles inside the aggregate. Moreover, special attention has been paid to other possible modes of the break up process, since we are interested in how and where the aggregates will break. The aggregate structure before break up was also investigated and compared for the different systems. The modeling has been developed further by also considering break up by erosion. With this model, the critical shear rate for break up by erosion was calculated as well as the kinetics of the erosion process.

The structure of the present paper is as follows. In Section 2, we present and discuss the results for the different experimental systems. In Section 3, a model for single particle erosion will be presented and compared with our experimental observations. The paper ends in Section 4 with a summary of our findings.

2. Experimental Observations

2.1. Materials and Methods. *2.1.1. Materials.* All measurements were conducted with spherical glass particles trapped at a liquid−fluid interface. A mixture of water with glycerol (35 wt %, Merck) was used as the lower liquid phase. Pentadecane (Merck) or air was used as the upper phase. In this way, two kinds of interfaces were created: a w/a and a w/o interface. Moreover, two sizes of glass particles were used: R_p = 115 μm and R_p = 65 μm (Polysciences,

(10) Pantina, J. P.; Fust, E. M. *Phys. Rev. Lett.* **2005**, *94*, 138301.
(11) Yeung, A. K.; Pelton, R. *J. Colloid Interface Sci.* **1996**, *184*, 579.
(12) Zhang, Z.; Sisk, M. L.; Mashmoushy, H.; Thomas, C. R. *Part. Part. Syst. Charact.* **1999**, *16*, 278.
(13) Stancik, E. J.; Gavranovich, G. T.; Widebrant, M. J. O.; Laschitsch, A. T.; Vermant, J.; Fuller, G. G. *Faraday Discuss.* **2003**, *123*, 145.
(14) Stancik, E. J.; Hawkinson, A. L.; Vermant, J.; Fuller, G. G. *J. Rheol.* **2004**, *48*, 159.
(15) Aveyard, R.; Clint, J. H.; Nees, D.; Paunov, V. N. *Langmuir* **2000**, *16*, 1969.
(16) Aveyard, R.; Clint, J. H.; Nees, D.; Quirke, N. *Langmuir* **2000**, *16*, 8820.
(17) Hoekstra, H.; Vermant, J.; Mevis, J. *Langmuir* **2003**, *19*, 9134.
(18) Hansen, P. H.; Malmsten, M.; Bergenstahl, B.; Bergstrom, L. *J. Colloid Interface Sci.* **1999**, *220*, 269.
(19) Bagster, D. F.; Tomi, D. *Chem. Eng. Sci.* **1974**, *29*, 1773.
(20) Adler, P. M.; Mills, P. M. *J. Rheol.* **1979**, *23*, 25.
(21) Sontag, R. C.; Russel, W. B. *J. Colloid Interface Sci.* **1987**, *115*, 378.
(22) Rumpf, H. *Agglomeration*; Knepper, W. A., Ed.; Wiley-Interscience: New York, 1962.
(23) Kendall, K. *Powder Metall.* **1988**, *31*, 28.
(24) Powel, R. L.; Mason, S. G. *AIChE J.* **1982**, *28*, 286.
(25) Pandya, J. D.; Spielman, L. A. *J. Colloid Interface Sci.* **1982**, *90*, 517.
(26) Vassileva, N. D.; van den Ende, D.; Mugele, F.; Mellema, J. *Langmuir* **2006**, *22*, 4959.

Table 1. System Properties[a]

system	upper phase	g [mN/m]	R_p [μm]	α_c [°]
w/a 115	air	71	115 ± 10	55 ± 2
w/o 115	pd	44	115 ± 10	54 ± 3
w/a 65	air	71	65 ± 10	41 ± 5
w/o 65	pd	44	65 ± 10	43 ± 5

[a] Lower phase is in all cases water/glycerol; pd = pentadecane.

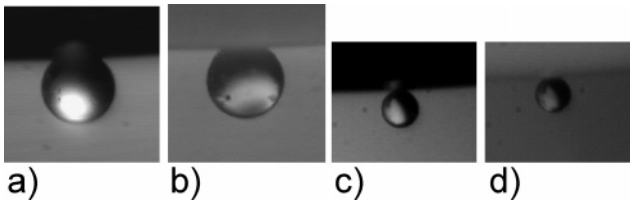

Figure 1. Images of a single particle positioned at the interface: (a) w/a 115, (b) w/o 115, (c) w/a 65, and (d) w/o 65.

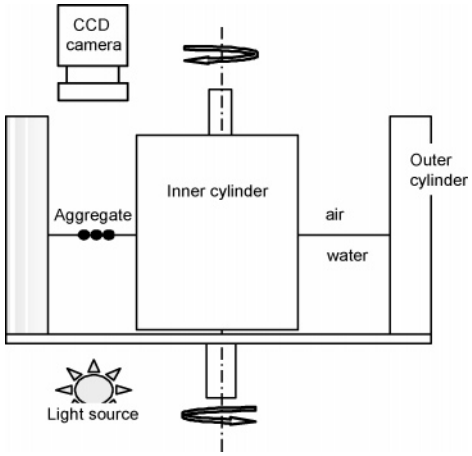

Figure 2. The experimental setup used in this study.

Inc., density 2480 kg/m^3). The glass particles were small enough to be trapped at the interface. The system properties are summarized in Table 1. The w/a 115 system was already discussed in our previous paper[26] and is mentioned here for comparison with the other systems. The lower phase has a viscosity of 2.34 mPa and a density of 1090 kg/m^3. Pentadecane also has a viscosity of 2.34 mPa and a density of 773 kg/m^3. For all systems, the particles were submerged mostly in the lower phase. Images of the particles positioned at the interface are shown in Figure 1, and the measured contact angles α_c are included in Table 1. Hereafter, the four investigated systems will be denoted according to the leftmost column of Table 1.

2.1.2. Setup and Procedure. The experimental setup, as illustrated in Figure 2, consists of a Couette device with two concentric cylinders ($R_i = 24$ mm, $R_o = 45$ mm) that can be rotated in opposite directions. This creates a controlled shear flow in the liquid confined by the gap between the cylinders, with a stagnant zone at a controllable radial position. Thin stainless steel rings were attached to the cylinders to create an edge at which the liquid−air interface is pinned. The flatness of the interface is controlled by adding or removing liquid to or from the lower phase and it is measured from the diffraction of a laser beam at the interface, as explained in ref 28.

The glass particles were added to the w/a interface. They aggregated fast due to the strong capillary attraction between them. In this way, the initial aggregate was created. For the w/o experiments, additionally, the oil phase is poured on the top of the water layer. It was checked that adding the oil phase does not affect the pinning of the three-phase contact line, keeping the liquid−liquid interface flat.

(27) Nikolaides, M. G.; Bausch, A. R.; Hsu, M. F.; Dinsmore, A. D.; Brenner, M. P.; Gay, C.; Weitz, D. A. *Nature* **2002**, *420*, 299.
(28) Vassileva, N. D.; van den Ende, D.; Mugele, F.; Mellema, J. *Langmuir* **2005**, *21*, 11190.

The interface is illuminated through the transparent bottom of the outer cylinder, while it is observed from above using a charge-coupled device (CCD) camera equipped with a zoom lens. The camera was connected to an image acquisition system. In principle, it is possible to keep the aggregate in the stagnant zone and thus in the field of view of the camera. However, the aggregate will stay at a fixed position only if the total shear forces on all particles cancel each other. When the aggregate rotates a little bit, due to its irregular shape, the shear forces change. Hence, in order to keep the aggregate at that position, the rotational speed of the cylinders should be adjusted continuously using a feedback loop, which, in practice, is not possible due to the relatively slow response of the flow field to the cylinder speed adjustments. This was observed by other researchers[18] as well. Instead, the aggregate is allowed to rotate slowly in the Couette device. The CCD camera is kept stationary, and the aggregate is recorded when it passes the field of view. The rotational speeds of the cylinders are set to minimize the velocity of the aggregate at the desired shear rate.

The protocol for measuring the restructuring and eventual break up of an aggregate was as follows: After the formation of the aggregate, it was sheared for 10 min at a fixed shear rate, starting at 0.1 s^{-1}, while images of the aggregate were captured. This time span was long enough to reach a steady state. After 10 min, the shear rate was increased in steps of 0.10 s^{-1} and again kept constant for 10 min. The highest applied shear rate was 2.5 s^{-1}, enough to observe break up of the aggregate.

2.1.3. Aggregate Characterization. The most relevant properties of the aggregate are the internal structure, size, and shape. The aggregate size is characterized by the number of particles, the shape is characterized by the aspect ratio L/B, where L is the largest diameter of the aggregate and B is the smallest, and the structure is characterized by the coordination number C_o as well as the Fourier transforms of the images. The coordination number represents the average number of nearest neighbors per particle inside the aggregate and has been calculated as explained in ref 26. All those characteristics were extracted from the recorded images using the image processing software tools Optimas and ImageJ, as has been explained in detail in Section 2.3 and in the appendix of ref 26.

2.1.4. Reproducibility. In general, the behavior of all aggregates from the four systems considered was qualitatively the same. It should be noted, however, that, for the same system, identical experiments sometimes produce different results. Considerable effort has been put into controlling the experimental conditions, as described in refs 26 and 28. Before each experiment, the whole setup was rigorously cleaned to prevent contamination by previous experiments. Also, the liquid−particle systems were allowed to equilibrate before the experiments were started as well as after each change in the shear rate. Still, some reproducibility problems remain. These can be due to dust from the ambient air, which, during the preparation of the experiment, can pollute the interface. These dust particles are difficult to observe since they are usually smaller than the particles. When dust is present at the interface, it will change the capillary interaction and thus the aggregate behavior. In the experiments, the temperature was not controlled, and the ambient temperature during the measurements was $T = 22 \pm 2$ °C. The variation in T is supposed to have only little influence on the aggregate behavior.

2.2. Results and Discussion. As mentioned in the introduction, we are interested in the structural changes and break up mechanisms of aggregates subjected to simple shear flow. First, we will consider the general aggregate behavior and the differences between the four investigated systems. Next, break up and its mechanisms will be studied in some detail. Eventually, the erosion kinetics, that is, the size evolution as a function of time, will be investigated.

2.2.1. General Aggregate Behavior. In Figure 3, representative images of aggregate behavior are shown at different shear rates for the four investigated systems. As one can see for all systems, in the initial stage the particles form compact, dense aggregates. With increasing shear rate, the aggregates become more circular, and the crystalline ordering increases in the center part of the aggregates while it decreases in the outer regions. At a certain, critical shear rate, the aggregate size is reduced significantly. The last image in

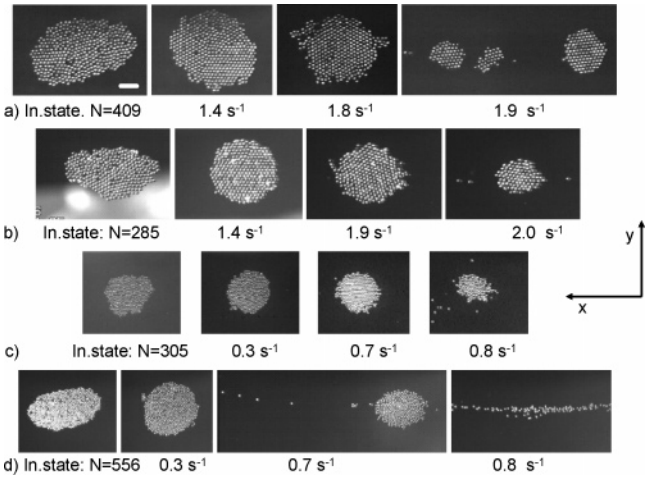

Figure 3. Images of the four investigated systems at different shear rates, as denoted below the photographs: (a) w/a 115, (b) w/o 115, (c) w/a 65, and (d) w/o 65. N is the initial number of particles inside the aggregate. The flow and the gradient direction are indicated by the x- and y-axes, respectively. The white bar in the upper left image corresponds to a length of 1 mm.

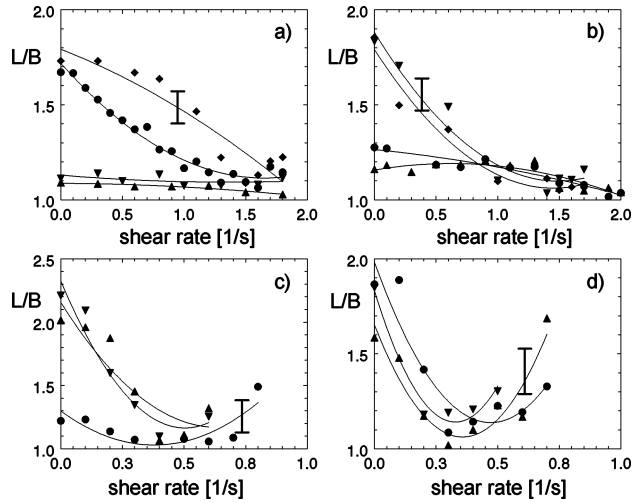

Figure 4. Typical aspect ratio L/B at different shear rates for (a) w/a 115 (from ref 26) with $N_i = 409$ (diamond), 198 (circle), 203 (down triangle), and 285 (up triangle); (b) w/o 115 with $N_i = 285$ (down triangle), 226 (diamond), 351 (circle), and 247 (up triangle); (c) w/a 65 with $N_i = 231$ (down triangle), 427 (up triangle), and 305 (circle); and (d) w/o 65 with $N_i = 556$ (circle), 284 (down triangle), and 413 (up triangle). The lines are a guide to the eye, and the error bars indicate the typical uncertainty due to statistics.

panel a (large particles system) clearly shows breaking by fragmentation, while, in panel d (smaller particles), the result of the erosion process is clearly visible.

2.2.1.1. Shape and Structure. In Figure 4, the aspect ratio has been plotted as a function of the shear rate. While the initial aspect ratio at $\dot{\gamma} = 0$ varies between 1 and 2.2, depending on the formation process of the aggregate, L/B is found to evolve toward 1 upon increasing the shear rate. Such increase in the circularity is characteristic for simple shear flow; it has not been observed in other types of flow, such as extensional flow.[13] We attribute this to the rotation of the aggregates. While the aggregates rotate as a result of the flow field, the particles near the end of the long axis are pushed aside by a tangential shear stress, which is larger than average, and hence, circular symmetry is promoted. However, when the shear rate approaches the critical shear rate, there is frequently a tendency toward larger aspect ratios at the onset of break up.

The evolution of the structure of an aggregate is characterized by changes in the coordination number C_o, and the Fourier images of the aggregates. In Figure 5, C_o has been plotted as a function of the

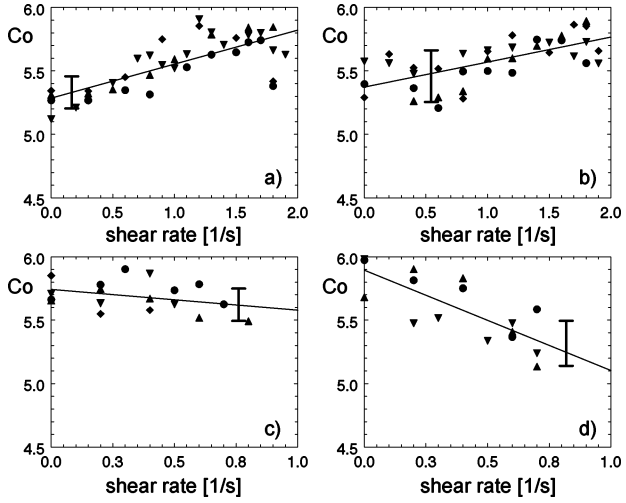

Figure 5. The coordination number as a function of the shear rate, measured for (a) w/a 115 (from ref 26) with $N_i = 409$ (circle), 203 (up triangle), 285 (diamond), and 191 (down triangle); (b) w/o 115 with $N_i = 285$ (circle), 226 (up triangle), 351 (down triangle), and 247 (diamond); (c) w/a 65 with $N_i = 1093$ (up triangle), 231 (down triangle), 427 (diamond), and 305 (circle); and (d) w/o 65 with $N_i = 782$ (down triangle), 556 (circle), and 413 (up triangle). The lines are a guide to the eye, and the error bars indicate the typical uncertainty due to statistics.

shear rate. There is a pronounced difference in the initial state between the systems with small and with large particles. For the w/x 65 systems (x stands for a or o) C_o is significantly larger in the initial state than it is for the w/x 115 systems. With increasing shear rate, the coordination number for w/x 65 systems is constant within the experimental accuracy (Figure 5c) or decreases (Figure 5d), while, for w/x 115, C_o increases (Figure 5a,b). Similar results for the coordination number as a function of the applied shear rate were obtained by Hoekstra et al.[17] for 2D suspensions. They observed for a system with a stronger attraction potential (a surfactant-free system) an increase in the coordination number with increasing shear rate, while a system with a weaker attraction potential (with surfactant) showed the opposite behavior, that is, a decrease in the coordination number with increasing shear rate. The two systems have a different bond strength between the particles. In the first one, the bonds are strong and, due to this normal force, the tangential friction forces are high, hence the particles cannot slide easily along each other, while, in the second system, the bonds are weaker and the particles can slide along each other.

The results for L/B and C_o as a function of $\dot{\gamma}$ show that, at low shear rates, an increase in the order and circularity of the aggregates is induced. At shear rates near the critical shear rate, a small decrease in both the circularity and the coordination number was observed in several experiments (Figures 4 and 5). This is again an indication that the aggregate structure starts to break down under the applied shear flow. The w/o 65 system also shows this decrease for low shear rates, which means that the flow destabilizes the aggregate at all shear rates.

The $C_o(\dot{\gamma})$ results indicate that all aggregates already had, or developed a crystalline structure. The large particle systems preferably develop a single-crystal structure, identified by the points in the 2D Fourier transform (Figure 6). The Fourier images of the small particle systems (one exception) showed the development of circular rings instead of points with increasing shear rate (Figure 7). The combination of a high coordination number with a ring structure in the Fourier images suggests the existence of multiple crystal domains with different orientations in the small particle system.

In ref 26, we argued that the w/a 115 aggregates behave as solid disc-like bodies. Compared to the motion of the aggregate as a whole, hardly any restructuring and movement of separate particles occurs inside the aggregate. This behavior is observed for the w/o 115 system as well, while w/x 65 aggregates become softer (i.e.,

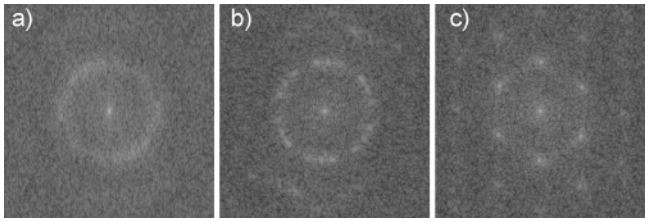

Figure 6. Evolution of the Fourier image of an aggregate for the w/o 115 system with $N_{in} = 285$ at (a) initial state, (b) shear rate 1 s^{-1}, and (c) 1.4 s^{-1}.

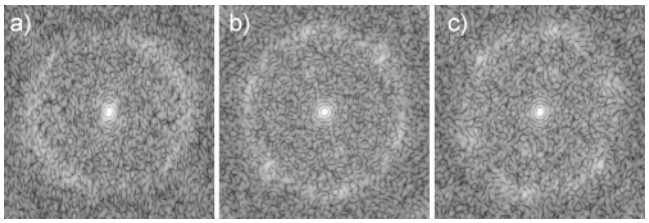

Figure 7. Evolution of the Fourier image of an aggregate for the w/o 65 system with $N_{in} = 413$ at (a) initial state, (b) shear rate 0.3 s^{-1}, and (c) 0.5 s^{-1}.

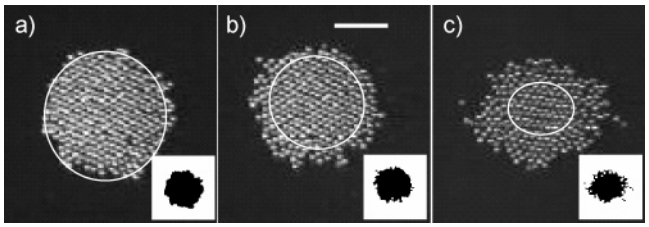

Figure 8. Formation of an disordered layer with increasing shear rate for w/a 65 at shear rates (a) 0.6 s^{-1}, (b) 0.7 s^{-1}, and (c) 0.8 s^{-1}. The initial number of particles was $N_{in} = 305$. The insets show a black and white transformation of the original images. The disordered layers are outside of the drawn ellipses. The white bar in the middle image corresponds to a length of 1 mm.

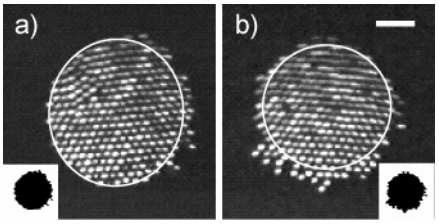

Figure 9. Formation of an disordered layer with an increasing shear rate for w/a 115 at shear rates (a) 1.5 s^{-1} and (b) 1.8 s^{-1}. The initial number of particles was $N_{in} = 285$. The insets show a black and white transformation of the original images. The disordered layers are outside of the drawn ellipses. The white bar in the right image corresponds to a length of 1 mm.

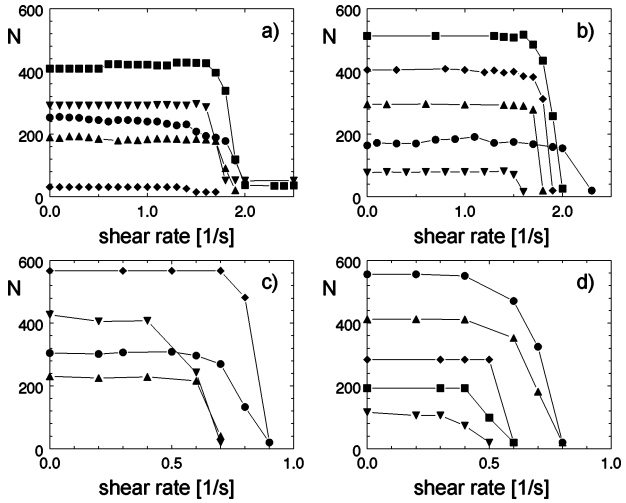

Figure 10. The number of particles as a function of the shear rate for (a) w/a 115, (b) w/o 115, (c) w/a 65, and (d) w/o 65 and several initial sizes.

more disordered) with increasing shear rate. In the initial stages of the experiment and at low shear rates ($\dot{\gamma} < 0.2$ s^{-1}), the aggregates have a hard crystalline structure. With increasing shear rate, a thin disordered layer forms along the edge of the crystalline core. At even higher shear rates, the thickness of the disordered layer grows. Just after increasing the shear rate above the critical shear rate, multiple disordered layers form, and eventually the outer layers start to erode very slowly. When the aggregate reduces in size, previously crystal layers, on the outside of the crystalline core, also become disordered. Thus the order/disorder boundary moves inward. The aggregate radius continues to reduce until an equilibrium radius is reached. In this situation, there is only a single disordered outer layer surrounding a multiple-domain, crystalline, circular-shaped core.

The formation of these multiple disordered layers has been illustrated in Figure 8 for a w/a 65 aggregate. The ellipses approximately indicate the boundary between the core and the outer layers. The insets in the figure are the same images in black and the white for better visualization of the more open disordered layer. It can clearly be seen that the core has a crystalline structure and that the outer layers are disordered. The video recordings clearly show that the particles in the disordered layer rearrange themselves continuously.

The large particle aggregates, which are supposed to behave as a solid body, develop only a narrow disordered layer (see Figure 9). The formation of a disordered layer around a crystalline core can be explained by considering friction forces. The friction force between two adjacent surfaces is proportional to the normal force acting on these surfaces. Inside an aggregate, the normal forces are largest in the central region of the aggregate, and the resulting friction forces will prevent the particles from sliding along each other. The friction forces on the outside of the aggregate are not that large, and hence the particles on the outside can slide and move around, resulting in a disordered outer layer. Due to the size of the particles, the normal forces and thus these friction forces are smaller for the w/*x* 65 systems, and a much thicker disordered layer will develop, just as observed in the experiments. In a transient situation, just after a stepwise change in shear rate, particles on the outside start eroding away, the aggregate becomes smaller, and both the normal forces and the friction forces inside the aggregate become smaller as well. As a consequence, the thickness of the disordered layer is more or less preserved while the aggregate reduces in size.

2.2.1.2. Size. The size of the aggregate is given by the number of particles. Representative experiments on the evolution of the aggregate size as a function of the shear rate are shown in Figure 10. As can be seen, the size stays more or less constant until the critical shear rate is reached. This critical shear rate, for all cases, depends only weakly on the aggregate size: $\dot{\gamma}_{cr} \simeq 1.9$ s^{-1} for the 115 μm particles, and $\dot{\gamma}_{cr} \simeq 0.7$ s^{-1} for the 65 μm particles.

However, every aggregate within each graph shows a little different critical shear rate. This must be due to small structural differences in the initial aggregates. In the next section, the critical shear rates, as observed in Figure 10, will be compared with model calculations.

2.2.1.3. Summary. The main differences between the systems have been summarized in Table 2. As can be seen, the aggregate behavior for the w/a and w/o interfaces is similar, but there is a significant difference in behavior between the large (115 μm) and small (65 μm) particle systems. The most important difference is the critical shear rate: for the small particle systems, it is about 2 times smaller than that for the large particle systems.

2.2.2. Break Up Mechanisms. First it has to be noticed that, due to their motion in the Couette apparatus, the aggregates are not permanent in the field of view of the camera. Hence, it is difficult to observe the aggregate break up directly. For example, if an

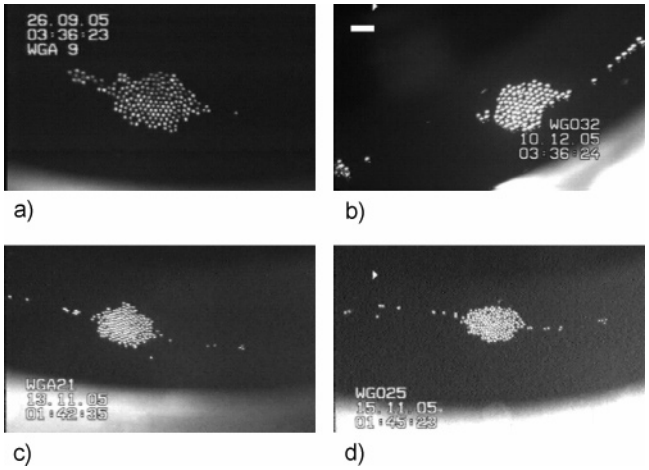

Figure 11. Direct observation of erosion for (a) w/a 115, at $\dot{\gamma} = 1.9\ s^{-1}$ with $N_{in} = 291$; (b) w/o 115, at $\dot{\gamma} = 2.1\ s^{-1}$ with $N_{in} = 222$; (c) w/o 65, at $\dot{\gamma} = 0.7\ s^{-1}$ with $N_{in} = 305$; and (d) w/a 65, at $\dot{\gamma} = 0.8\ s^{-1}$ with $N_{in} = 556$. The white bar in the upper right image corresponds to a length of 1 mm.

Table 2. Summary of the Differences between the Experimental Systems

system	$\dot{\gamma}_{cr}$, s^{-1}	initial C_o	structure
w/a 115	1.9 ± 0.1	5.4 ± 0.6	mostly single domain crystal small disordered layer
w/o 115	1.9 ± 0.3	5.2 ± 0.4	single domain crystal or with defects, small disordered layer
w/a 65	0.8 ± 0.1	5.7 ± 0.1	multidomain crystal, hard ($\leq 0.6\ s^{-1}$) and soft ($> 0.6\ s^{-1}$) disordered layer increases with $\dot{\gamma}$
w/o 65	0.6 ± 0.2	5.8 ± 0.2	multidomain crystal, hard ($\leq 0.3\ s^{-1}$) and soft ($> 0.3\ s^{-1}$) disordered layer increases with $\dot{\gamma}$

aggregate returns into the field of view in several pieces, it is not obvious whether it fragmented, or eroded and afterward reaggregated during the time that it was not visible. The mechanism of break up was determined from the direct observations in front of the camera and from indirect indications such as the size of the aggregate as a function of time or the presence of free particles in the system. We observed both erosion and fragmentation in the experiments. We consider the two mechanisms separately.

2.2.2.1. Break Up by Erosion. In Figure 11 and in Figure 3c,d, one can see single particles eroding. If one considers the size distribution of the aggregates after break up, the erosion seems more pronounced for the small particle systems (see the images in Figure 3). For these systems, there are a lot of free particles present, as can be observed from Figure 3d. When the size distribution after break up contains mainly free particles, this is a strong indication of erosion. However, the eroded particles can form new aggregates again, hence the presence of small aggregates after break up is not inconsistent with erosion.

Another argument for erosion is given by the time dependence of the aggregate size. Erosion will show a continuous decrease in time, while fracture is a discontinuous, stepwise reduction of the aggregate size. As we will discuss in Section 3.4, in most cases, a gradual decrease has been observed (see Figure 15), indicating break up by erosion.

2.2.2.2. Break Up by Fragmentation. Figure 12 shows consecutive images of the break up process. On the video recordings, it can be seen that the separate fragments of the aggregate move independently from the main aggregate. In the static pictures, this temporal information has been lost, and the separate pieces appear to still be attached, but they are not. The last frames show the daughter aggregates when break up has been completed. Break up in fragments in front of the camera was not observed for the small particle systems. The fragmentation occurs in the outer regions of the aggregate, as

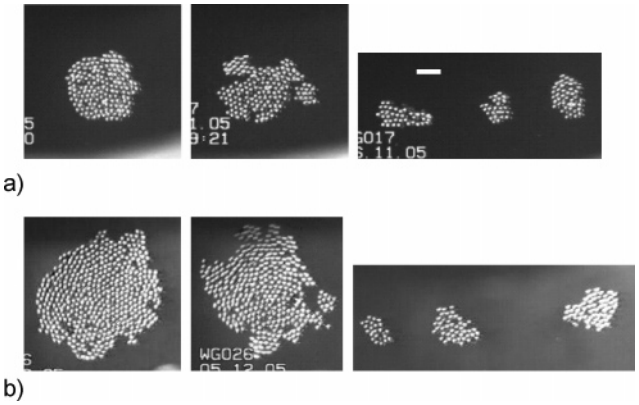

Figure 12. Breaking in the field of view for the w/o 115 system. Case a corresponds to $N_{in} = 164$ at $\dot{\gamma} = 2.2\ s^{-1}$, and case b corresponds to $N_{in} = 449$ at $\dot{\gamma} = 1.3\ s^{-1}$. The first frame shows the aggregate before it breaks, while the last frame shows the broken aggregate the next time it passes the field of view. The white bar in the upper right image corresponds to a length of 1 mm.

can be seen in Figure 12, and the aggregate breaks in more than two parts. It was also noticed that the fragmentation starts with a single rupture. Rupture of the first fragment triggers more rupturing processes. This cascade of fragmentation can be explained from the fact that the aggregate loses it circular shape and thus becomes weaker once the first part has been broken.

The critical shear rate for the two cases in Figure 12 is quite different, that is, $2.2\ s^{-1}$ for the first case and $1.3\ s^{-1}$ for the second case. This is partially due to the statistical nature of the break up process, but it is also due to the aggregate size dependence of the critical shear rate. For instance, large aggregates can contain more defects that will promote the fragmentation. For the aggregates shown in Figure 12, the break up occurred about 1−2 min after applying the shear rate, which is much faster than the processes in Figure 11.

In summary, break up by both erosion and fragmentation has been observed. Single-particle erosion is the prevailing process. As it was shown in Figure 3c,d, the critical shear rates for fragmentation and erosion are similar, and the aggregates can break by both mechanisms. We have indications that fragmentation is promoted by the presence of defects in the crystal structure. The analysis of the video images clearly showed that aggregates with a perfect hexagonal structure will break by erosion due to the stronger bonding between the particles in the inner regions of the aggregate.[11] Due to the large normal and friction forces, restructuring in the large particle systems is more difficult than in the small particle systems. Aggregates from the latter systems restructure easier with the applied flow, which is consistent with a preferential break up by erosion.

3. Modeling Break Up by Erosion

In our previous paper,[26] the critical shear rate for break up by fragmentation was modeled. In this section, we model the critical shear rate for break up by erosion as well as the time evolution of the aggregate size due to erosion. Next, we confront the model calculations with the experimental results just described.

3.1. Interaction Forces. For colloidal 2D systems, interaction forces include capillary, van der Waals, electrostatic, excluded volume repulsion, and electric-field-induced capillary[27] forces. Due to the size of the primary particles, the gravity-driven capillary interaction in our system is so strong that all other interaction forces, except the excluded volume repulsion, can be neglected. As discussed in ref 28, in the "linear superposition approximation" (LSA), the capillary force between particles *a* and *b* is given by

$$F_{LSA}^{[a,b]} = 2\pi\sigma q Q^2 K_1(q r_{ab}) \quad (1)$$

where $K_1(x)$ is the modified Bessel function of first order, and

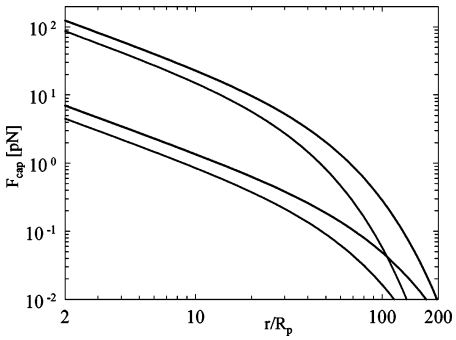

Figure 13. Calculated capillary force between two particles for the four systems investigated. From top to bottom: w/o 115, w/a 115, w/o 65, and w/a 65.

r_{ab} is the distance between particles a and b.[29,30] The coefficient Q is defined as $Q = r_{cl} \sin \psi$, where r_{cl} is the radius of the three-phase contact line around the particle, and ψ is the angle between the liquid interface and the horizontal plane near the particles. The inverse capillary length is given by $q = (g\Delta\rho/\sigma)^{1/2}$, where g is the acceleration due to gravity, $\Delta\rho$ is the density difference between the lower and upper liquids, and σ is the surface tension. In ref 28, we showed that the LSA expression is also valid at short distances between the particles as a consequence of the multiparticle interactions being pairwise additive.

In Figure 13, the capillary force between two particles has been plotted for the investigated systems. For small r/R_p values, the force scales with $1/r$. For large r/R_p values, the force scales with $\sqrt{\pi/2qr}\exp(-qr)$. The transition at $qr \simeq 2$, and hence the reach of the interaction, depends on the system $r/R_p = 45$, 60, 80, and 115 for w/a 115, w/o 115, w/a 65, and w/o 65, respectively.

Apart from this central capillary force, friction between two touching particles can occur. This friction can be dynamic (sliding) or static (sticking). The distinction is important because the dynamic friction can be significantly smaller than the static friction. This friction force is considered to be proportional to the normal force with which the surfaces are pushed together. In the inner regions of an aggregate, the normal forces are larger than those in the outer regions, due to the long-range tail of all two-particle interactions in the environment of the considered particle pair, and hence the friction forces are also larger in the inner regions.

3.2. Flow Field. A particle moving in an interface between two liquids experiences a drag force due to the presence of the two liquids and the interface itself. Hence, we modify the Stokes drag force by introducing an additional f_d coefficient:

$$F_d = 6\pi\mu R_p f_d V \qquad (2)$$

where μ is the viscosity of the lower phase, R_p is the particle radius, and f_d is a friction coefficient on the order of unity to account for the partial immersion of the particle in the lower phase and the hydrodynamic screening of the other particles in the aggregate.[26] V is the local undisturbed flow velocity, relative to the particle. The nature of the flow also influences the fragmentation process. In simple shear flow, significantly higher shear rates are required for break up compared to extensional flow.[31] In general, the less vorticity there is in a flow, the more efficient is the break up.[32] On the other hand, simple shear flow can be more efficient than extensional flow if rupture is occurring along a crack line. Due to the rotational motion of the aggregates, the crack line will pass through certain orientations that are favorable for aggregate break up.[33]

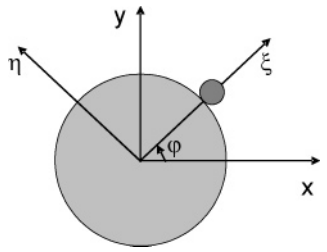

Figure 14. The scheme used for modeling the erosion of a single particle.

The flow field around a particle in an aggregate is disturbed by its neighboring particles. This hydrodynamic contribution can give rise to both normal and tangential forces on the particles. In a system with just two particles, it leads to an effective repulsive force between approaching particles and can prevent them from aggregation. In our 2D system, there is a more or less free flow above and below the particles, and, in first approximation, the hydrodynamic force on an individual particle can be modeled as a simple Stokes law, as for isolated particles.

The influence of the Brownian motion can be neglected in our noncolloidal system, while inertia forces have been calculated to be significantly smaller than the interaction and drag forces.

3.3. Critical Shear Rate for Erosion. The critical shear rate for erosion can be calculated using the formalism explained in ref 26 with some small adjustments. We consider a disc-shaped aggregate with radius R and a single particle on its rim, as illustrated in Figure 14.

To predict break up in this case, again both the capillary and the hydrodynamic force have to be calculated. The capillary force between aggregate A and particle b can be calculated by summing the particle−particle interactions between every particle in A with particle b. Using eq 1 for the two-particle interaction, the capillary force $dF^{[c]}$ between a small area element dA located at ($r\cos\beta$, $r\sin\beta$) and particle b located at ($R + R_p$,0) in the (ξ,η) frame, is given by

$$dF^{[c]} = 2\pi\sigma q Q^2 K_1(qr_{ab}) n dA$$

where $r_{ab} = [(R + R_p - r\cos\beta)^2 + (r\sin\beta)^2]^{1/2}$ is the distance between dA and the particle. The number of particles per unit area is given by $n = (2\sqrt{3}R_p^2)^{-1}$, assuming hexagonal packing.

To sum the interactions of every element dA in A with the particle b, one has to integrate over the area of the aggregate. For the components of the force $dF^{[c]}$ in the ξ- and η-direction, we have

$$F_\xi^{[c]} = C_1 \int_0^{2\pi} \int_0^R K_1(qr_{ab}) \cos\theta \, r dr d\beta$$

$$F_\eta^{[c]} = C_1 \int_0^{2\pi} \int_0^R K_1(qr_{ab}) \sin\theta \, r dr d\beta$$

where $C_1 = 2\pi\sigma q Q^2 n$ is a constant and

(29) Chan, D. Y. C.; Henry, J. D.; White, L. R. *J. Colloid Interface Sci.* **1981**, *79*, 410.
(30) Kralchevsky, P. A.; Nagayama, K. *Langmuir* **1994**, *10*, 23.
(31) Manas-Zloczower, I.; Feke, D. L. *Int. Polym. Process. II* **1988**, *3*−*4*, 185.
(32) Van de Ven, T. G. M. *Colloidal Hydrodynamics*; Academic Press: London, 1989.
(33) Feke, D. L.; Manas-Zloczower, I. *Chem. Eng. Sci.* **1991**, *46*, 2153.

$$\tan\theta = \frac{r\sin\beta}{R + R_p - r\cos\beta}$$

We assume that the hydrodynamic force on particle *b* is just the drag force, as given by eq 2. In simple shear flow, the velocity is given by $V = \dot{\gamma} y e_x$. This flow can be decomposed into a straining flow and a rotation:[32]

$$V = \frac{1}{2}\dot{\gamma}(ye_x + xe_y) + \frac{1}{2}\dot{\gamma}(ye_x - xe_y)$$

Since the aggregate can follow the rotation, this component of the flow does not exert any force on the aggregate. Eventual break up of the aggregate stems from the straining flow field. Therefore, we only consider this component in the calculations (the first term on the right-hand side). Because the force should be calculated in the body fixed (ξ,η) coordinate system, the (x,y) components of this straining field and the resulting drag force on particle *b* are expressed in the (ξ,η) components:

$$F_{\xi}^{[d]} = 3\pi\mu R_p f_d \dot{\gamma}(\xi \sin 2\varphi + \eta \cos 2\varphi)$$

$$F_{\eta}^{[d]} = 3\pi\mu R_p f_d \dot{\gamma}(\xi \cos 2\varphi - \eta \sin 2\varphi)$$

where φ is the angle between the ξ and x directions. The total drag force on part *A* should be equal but opposite to that on particle *b*. The extensional drag force is maximum for $\varphi = 45°$. Due to symmetry, both $F_{\eta}^{[c]}$ and $F_{\eta}^{[d]}$ are zero in this case, and we can express the critical shear rate from a force balance

$$3\pi\mu R_p f_d \dot{\gamma}_{crit}(R + R_p) = C_1 \int_0^{2\pi}\int_0^R K_1(qr_{ab})\cos\theta\, r dr d\phi$$

as

$$\dot{\gamma}_{crit} = \frac{\sigma q Q^2}{3\sqrt{3} f_d \mu R_p^3} \frac{\int_0^{2\pi}\int_0^R K_1(qr_{ab})\cos\theta\, r dr d\phi}{(R + R_p)} \qquad (3)$$

The integral expression for the critical shear rate (eq 3) has been evaluated numerically, where $\dot{\gamma}_{crit}$ was expressed as a function of *N*, that is, the number of particles inside the aggregate; *N* is related to the radius of the aggregate *R* (assuming close hexagonal packing) by

$$N = \frac{\pi}{2\sqrt{3}}\left(\frac{R}{R_p}\right)^2$$

The critical shear rate for erosion, assuming $f_d = 1$, has been calculated for the two different systems studied here: small and large particles. The viscosity and interfacial tension values are taken for the w/a interface. The results are presented in Figure 15.

For comparison the critical shear for fragmentation in two halves (as calculated in our previous paper, eq 14 in ref 26) is also presented in the figure. As can be seen, the small particle aggregates will erode or fragment at a much lower shear rate than the large particle aggregates. The dependence of the critical shear rate on the size of the aggregate is small, especially for the small particle system. Surprisingly, the critical shear rates for breaking by erosion or fragmentation are very close to each other. Hence, one can expect the aggregates to break by both mechanisms. One has to keep in mind that we only have an order of magnitude guess for the value of f_d. For $f_d \neq 1$, we can read the vertical axis in Figure 15 as $f_d\dot{\gamma}_{crit}$ to obtain the dependence of $\dot{\gamma}_{crit}$ on f_d.

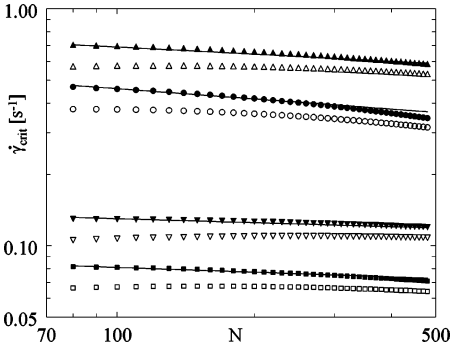

Figure 15. Calculated critical shear rate for the erosion of single particles or fragmentation into two equal parts for w/o 115 (up triangles), w/a 115 (circles), w/o 65 (down triangles), and w/a 65 (squares). The closed symbols represent the critical shear rate for fragmentation, the open symbols are for erosion. The lines are a fit, according to eq 6.

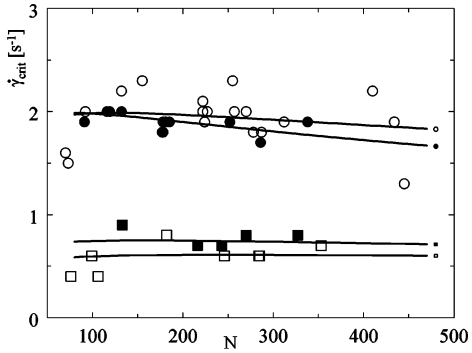

Figure 16. Critical shear rate versus the number of particles for the different systems. Solid circles: w/a 115; open circles: w/o 115; solid squares: w/a 65; open squares: w/o 65. The lines are fits according to eq 3 with $f_d = 0.19$, 0.29, 0.09, and 0.18 for w/a 115, w/o 115, w/a 65, and w/o 65, respectively.

In Figure 16 the critical shear rates for all experiments are summarized. They have been compared with the calculated critical values, using the model for break up by erosion, eq 3. The model for break up by fragmentation should give comparable results, as can be concluded from Figure 15. The lines in Figure 16 represent the calculations. Only one fitting parameter was used: f_d. The best fits were found for $f_d = 0.19 \pm 0.01$ (0.29 ± 0.04) in the case of w/a 115 (w/o 115) and $f_d = 0.09 \pm 0.01$ (0.18 ± 0.06) in the case of w/a 65 (w/o 65). Due to the scattering in the experimental data, the uncertainty in f_d is quite large. These f_d values are smaller than expected for two-particle interactions where we found $f_d = 1.2$ for w/o systems.[28] This can be attributed to the hydrodynamic screening of the particle at the rim by its neighbors inside the aggregate, which lowers the effective drag force on the particle and thus the value of f_d. The drag force on a fully immersed particle (in the case of the w/o systems) is still significantly larger than on a partially immersed particle (in the case of the w/a systems) at the same flow strength. Because the interparticle force for the w/o system is also about 50% larger than the corresponding w/a system (see Figure 13), the critical shear rates for aggregates at a w/a and a w/o interface are almost the same.

3.4. Modeling the Erosion Kinetics. We are also interested in the number of particles *dN* inside an aggregate that escape from the aggregate during *dt* or, equivalently, the time rate of change of the aggregate radius *R*:

$$\frac{dN}{dt} = \frac{d}{dt}\frac{\pi R^2}{2\sqrt{3}R_p^{\,2}} = \frac{\pi R}{\sqrt{3}R_p^{\,2}}\frac{dR}{dt} \tag{4}$$

To simplify the argument, we assume that the average escape rate Y for a single particle will be given by

$$Y = c_1(F_{hydr} - F_{attr})_{max}$$

where c_1 is a constant. The total escape rate dN/dt should be proportional to the number of particles at the rim of the aggregate, $N_{rim} = \pi R_{agg}/R_p$:

$$\frac{dN}{dt} = -\frac{\pi R}{R_p}Y = -c_1\frac{\pi R}{R_p}(F_{hydr} - F_{attr})_{max} \tag{5}$$

In the preceding section, we calculated the critical shear rate for break up by erosion. From that we can express the maximal attraction force as

$$F_{attr} = 3\pi\mu f_b (R + R_p) R_p \dot{\gamma}_{crit}$$

while the maximal hydrodynamic force is given by

$$F_{hydr} = 3\pi\mu f_b (R + R_p) R_p \dot{\gamma}$$

So, using eq 4, eq 5 can be written as

$$\frac{dR}{dt} = -c(R + R_p)(\dot{\gamma} - \dot{\gamma}_{crit})$$

with $c = 3\sqrt{3}c_1\pi\mu f_b R_p^{\,2}$ being a dimensionless constant. To simplify the calculation, we describe the dependence of $\dot{\gamma}_{crit}$ on the aggregate size as a power law:

$$\dot{\gamma}_{crit} = \dot{\gamma}_0\left(\frac{R}{R_p}\right)^{-2/k} = \dot{\gamma}_0\frac{2\sqrt{3}}{\pi}N^{-1/k} \tag{6}$$

As shown in Figure 15, this power law is in reasonable agreement with the analytical model for $k \simeq 10$ for the 115 μm particles and $k \simeq 15$ for the 65 μm particles. The differential equation that one has to solve becomes

$$\frac{d}{dt}\left(\frac{R}{R_p}\right) = -c\left(\frac{R}{R_p} + 1\right)\left(\dot{\gamma} - \dot{\gamma}_0\left(\frac{R}{R_p}\right)^{-2/k}\right)$$

The steady-state solution of this equation is given by

$$R_\infty = R_p\left(\frac{\dot{\gamma}}{\dot{\gamma}_0}\right)^{-k/2}$$

with R_∞ being the radius of the aggregate for $t \to \infty$. This could also be concluded directly from eq 6. Assuming $R/R_p \gg 1$, one obtains for the differential equation

$$c\dot{\gamma}t = \int_{z(t)}^{z_0}\frac{dz}{z(1 - z^{-2/k})} = \frac{k}{2}\ln\left(\frac{z_0^{2/k} - 1}{z^{2/k}(t) - 1}\right)$$

where $z = R/R_\infty = (N/N_\infty)^{1/2}$, and $z_0 = z(t = 0)$. This relation can be inverted to

$$z(t) = [1 + (z_0^{2/k} - 1)\exp(-2c\dot{\gamma}t/k)]^{k/2}$$

Hence, one eventually obtains for the aggregate size as a function of time

$$N(t) = [N_\infty^{1/k} + (N_0^{1/k} - N_\infty^{1/k})\exp(-2c\dot{\gamma}t/k)]^k \tag{7}$$

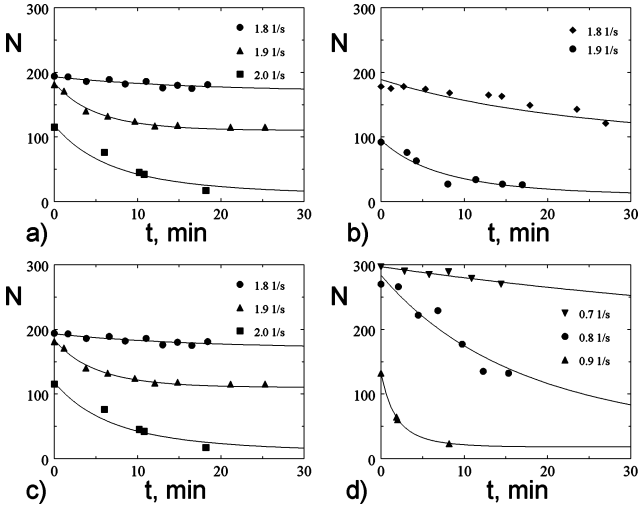

Figure 17. Number of particles in an aggregate as a function of time for (a,b) w/a 115, (c) w/o 115, and (d) w/a 65. The symbols represent the experimental data, and the lines represent the fit according to the model, eq 7. The shear rates are shown in the graphs.

Table 3. Summary of the Fitting Constants[a]

system	$\dot{\gamma}$, s^{-1}	N_0	k	$\dot{\gamma}_0$, s^{-1}	N_∞ calc	c fit	N_∞ fit
(a) w/a 115	1.8	194			133	0.260	170
	1.9	181	17	2.4	53	0.738	110
	2.0	115			22	0.243	10
(b) w/a 115	1.8	178	17	2.4	133	0.138	89
	1.9	92			53	0.255	8
(c) w/o 115	1.8	229	17	2.3	64	0.015	78
	1.9	224			25	0.063	4
(d) w/a 65	0.7	297			510	0.576	156
	0.8	270	34	0.9	55	0.419	17
	0.9	132			1	4.719	18

[a] k and $\dot{\gamma}_0$ were obtained from Figure 16, and N_∞ (calc) was calculated with eq 8, while c and N_∞ (fit) resulted from Figure 17.

where N_0 is the number of particles inside the aggregate at $t = 0$, when the shear rate was set to $\dot{\gamma}$.

In Figure 17, the experimentally obtained time dependence of the aggregate size has been given for the w/a 115, w/o 115, and w/a 65 systems. Although the data scatter a little, the typical transient times and the final values for N_∞ can still be estimated from these curves. N_∞ decreases strongly with increasing shear rate, in agreement with the critical shear rates plotted in Figure 16, while the characteristic decay time also seems to decrease with increasing shear rate.

To compare the measured size evolution with the model just derived (eq 7), the constants N_∞ and c were used as fitting parameters. The optimum k value was found (together with $\dot{\gamma}_0$) by fitting eq 6 to the critical shear rate as a function of the number of particles, as given in Figure 16. For particles with a radius of 115 μm, the optimum k value is 17, while, for particles with a radius of 65 μm, this value is 34. N_0 is the initial number of particles in the aggregate. The fitted value for N_∞ can be compared with the prediction based on eq 6:

$$N_\infty = \frac{\pi}{2\sqrt{3}}(\dot{\gamma}/\dot{\gamma}_0)^{-k} \tag{8}$$

The only unknown is the dimensionless constant c. Also, the model fits are plotted in Figure 17. They describe the experimental data reasonably well. The resulting values for the fitting parameters are presented in Table 3, where k and $\dot{\gamma}_0$ have been

obtained from fits to the data in Figure 16, while c and N_∞ resulted from Figure 17.

From the table we observe that the fitted values for N_∞ correlate, but not perfectly, with the values found with eq 8. The values for c scatter quite a lot for the different shear rates. The model implies that the c value should be the same for each experiment within the same experimental system. However, there is no trend visible in the deviations of N_∞, nor in c. Thus, the model cannot be completely validated. A possible explanation for the scattering in c values could be that the real break up mechanism consists of a mixture of fragmentation and erosion instead of just pure erosion. Erosion is dominant in the measurements that fit the model reasonably well (Figure 17a,d).

4. Conclusions

Break up by both erosion and fragmentation has observed. Erosion was observed in all investigated systems, while fragmentation was seen only for the large particle systems. According to the calculations, the critical shear rates for erosion and fragmentation are similar, thus both mechanisms can occur simultaneously. We have shown examples where break up in fragments was initiated by the presence of defects in the aggregate structure. No differences in behavior have been observed between the w/a and w/o systems, but the differences between the large and small particle systems were significant. They differ in critical shear rate, coordination number, and orientational ordering, as shown by the Fourier images. These differences can be understood by noting that the normal forces in the center of the aggregate are larger than those near its rim. These normal forces and thus (as we assume) the resulting friction forces are larger for the larger particle systems. Hence, restructuring in the central part of the large particle aggregates is hardly possible, and fracturing initiated by crack growth is favored. In the small particle aggregates, this restructuring is feasible, and so crack growth is unlikely, while erosion far inside the aggregate is possible. However, analytical modeling of these friction forces is very difficult, and we propose for future work to use numerical simulation techniques to model our experimental system in order to gain more insight in the influence of friction forces on the aggregate behavior in a shear flow and possibly to support our conclusions here.

The critical shear rate for break up by fracturing or erosion could be described by our model calculations, assuming a quite low value for f_d. This low f_d value can be attributed to the hydrodynamic interaction with neighboring particles, which, at contact, lowers the net drag force on the particle. Also, the time evolution of the aggregate sizes after a step increase in shear rate was reasonably well described by our model calculations.

Acknowledgment. This work has been supported by the Foundation for Fundamental research on Matter (FOM), which is financially supported by the Netherlands Organization for Scientific Research (NWO).

LA0625087